Reexamination of the Wave Activity Envelope Convective Scheme in Theoretical Modeling of MJO

GUOSEN CHEN

Earth System Modeling Center, Nanjing University of Information Science and Technology, Nanjing, China, and Department of Atmospheric Sciences and International Pacific Research Center, University of Hawai'i at Mānoa, Honolulu, Hawaii

BIN WANG

Department of Atmospheric Sciences and International Pacific Research Center, University of Hawai'i at Mānoa, Honolulu, Hawaii, and Earth System Modeling Center, Nanjing University of Information Science and Technology, Nanjing, China

(Manuscript received 19 April 2016, in final form 20 October 2016)

ABSTRACT

The skeleton model is one of the theoretical models for understanding the essence of the Madden–Julian oscillation (MJO). The heating parameterization scheme in the skeleton model assumes that precipitation tendency is in phase and proportional to the low-level moisture anomaly. The authors show that the observed MJO precipitation tendency is not in phase with the low-level moisture anomaly. The consequence of the wave activity envelope (WAE) scheme is reexamined by using a general MJO theoretical framework in which trio-interaction among convective heating, moisture, and wave–boundary layer (BL) dynamics are included and various simplified convective schemes can be accommodated. Without the BL dynamics, the general model framework can be reduced to the original skeleton model. The authors show that the original skeleton model yields a neutral mode that exhibits a "quadrupole" horizontal structure and a quadrature relationship between precipitation and low-level moisture; both are inconsistent with observations. With the BL dynamics and damping included, the model can produce a growing mode with improved horizontal structure and precipitation–moisture relationship, but deficiencies remain because of the WAE scheme. The authors further demonstrate that the general model with the simplified Betts–Miller scheme and BL dynamics can produce a realistic horizontal structure (coupled Kelvin–Rossby wave structure) and precipitation–moisture relationship (i.e., the BL moisture convergence leads precipitation, and column-integrated moisture coincides with precipitation).

1. Introduction

The MJO skeleton model has been considered a cornerstone for the MJO theory (Majda and Stechmann 2009, hereafter MS09). The skeleton model provides a simple way to understand the slow eastward propagation and peculiar dispersion feature of the MJO. However, the original skeleton model only produces neutral modes that can propagate both eastward and westward; therefore, the skeleton cannot explain the predominant eastward propagation and unstable growth of the MJO over the warm ocean as observed by Wang and Rui (1990b). To remedy these deficiencies, Liu and Wang (2012) extended the skeleton model by including boundary layer (BL) dynamics. The resulting "frictional skeleton model" produced unstable planetary-scale eastward-propagating modes and damped westward-propagation modes so that the BL moisture convergence provides a preferred eastward propagation and planetary-scale instability. Their results also illustrate that BL moisture convergence leads the convection, which is consistent with the observations (Hendon and

Salby 1994; Sperber 2003; Hsu and Li 2012). On the other hand, Thual et al. (2014) extended the MJO skeleton model by adding the "muscles," which was presented by stochastic parameterization of the unresolved synoptic activity. This skeleton model with muscles could explain intermittent generation of MJO events.

Despite the success of the skeleton and frictional skeleton models in interpreting some essential aspects of the MJO, some underlying caveats and limitations exist that deserve further investigation. The key premise of the skeleton model is that the MJO precipitation is proportional to the so-called (synoptic) wave activity envelope (WAE), and the WAE is assumed to grow (decay) over regions of a positive (negative) low-level moisture anomaly. Many previous studies have found that the MJO moisture field has westward vertical tilt and leads the major MJO convection anomalies in the lower troposphere or the boundary layer (Hendon and Salby 1994; Maloney and Hartmann 1998; Sperber 2003; Tian et al. 2006; Benedict and Randall 2007; Adames and Wallace 2015; Jiang et al. 2015). Many observational studies have also shown that water vapor (and relative humidity) is basically in phase with convective activity (Johnson and Ciesielski 2013; Powell and Houze 2013; Sobel et al. 2014; Xu and Rutledge 2014; Adames and Wallace 2015). However, the WAE's assumption that the precipitation tendency is proportional to the low-level moisture has not been rigorously tested against observations. It is not known whether this assumption adequately describes the observed phase relationship between precipitation and moisture distributions.

In the present study, we will first examine the adequacy of the WAE assumption using observational data and then investigate the consequences of this assumption using a general theoretical model framework for describing essential dynamics of the MJO (Wang and Chen 2016). This general theoretical framework integrates the processes described in previous theoretical models, such as the wave–conditional instability of the second kind (CISK) (Lau and Peng 1987), wind–evaporation feedback (Emanuel 1987; Neelin et al. 1987; Wang 1988a), frictional moisture convergence (FC) feedback (Wang 1988b; Wang and Rui 1990a; Wang and Li 1994; Kang et al. 2013), moisture–convective heating feedback (Sobel and Maloney 2012, 2013; Wang and Chen 2016), and the wave activity–driven multiscale interaction mechanisms (Wang and Liu 2011; Liu and Wang 2012). In this sense, it is a general model framework that could incorporate major ingredients of existing theoretical models. This model can also accommodate a variety of cumulus

parameterization schemes, such as the simplified Betts–Miller (B–M) scheme (Betts and Miller 1986; Betts 1986) and the Kuo scheme (Kuo 1974). Given the success of the model in simulating fundamental physical features of the MJO, it is worth incorporating the WAE parameterization scheme into this general MJO model to see if the solutions can produce essential features of the MJO.

The rest of the paper is outlined as follows. Section 2 describes the general MJO theoretical framework and the data used. Section 3 presents the observed relation between moisture and precipitation and the observed horizontal structure of the MJO. The effect and deficiency of the WAE convective scheme is reexamined using the general model in section 4. Section 5 compares the simulated MJO structures by using the general MJO model with the simplified Betts–Miller scheme. Conclusions and discussion are given in section 6.

2. Model and data

a. The general MJO model

The model consists of a baroclinic mode of the free atmospheric motion and barotropic BL dynamics. The model extends the Matsuno–Gill theory (Matsuno 1966; Gill 1980) by incorporating the trio-interaction among convective heating, moisture, and wave–BL dynamics. The model framework consists of a 1.5-layer equatorial beta-plane model (Wang and Chen 2016). Using horizontal velocity scale C_0, length scale $(C_0/\beta)^{1/2}$, time scale $(\beta C_0)^{-1/2}$, geopotential scale C_0^2, and moisture scale $d_0 \Delta p/g$, the nondimensional equations for the general MJO model are

$$\frac{\partial u}{\partial t} - yv = -\frac{\partial \Phi}{\partial x} - \nu u, \tag{1}$$

$$\frac{\partial v}{\partial t} + yu = -\frac{\partial \Phi}{\partial y} - \nu v, \tag{2}$$

$$\frac{\partial \Phi}{\partial t} + D + dD_b = -\mathrm{Pr} - \mu\Phi, \tag{3}$$

$$\frac{\partial q}{\partial t} + \overline{Q}D + \overline{Q}_b dD_b = -\mathrm{Pr}, \tag{4}$$

$$\frac{\partial u_b}{\partial t} - yv_b = -\frac{\partial \Phi}{\partial x} - E_k u_b, \quad \text{and} \tag{5}$$

$$\frac{\partial v_b}{\partial t} + yu_b = -\frac{\partial \Phi}{\partial y} - E_k v_b. \tag{6}$$

Equation (3) is the combined hydrostatic, continuity, and thermodynamic equation, while Eqs. (1) and (2) are momentum equations. Equation (4) is the vertically integrated moisture equation. Equations (5) and (6) are momentum equations for the barotropic BL. The

TABLE 1. Parameters and their standard values used in the model.

Parameter	Description	Typical value utilized here
Δp	Half-pressure depth of the free atmosphere	400 hPa
P_s	Pressure at the surface	1000 hPa
P_e	Pressure at BL top	900 hPa
P_2	Pressure at level 2	500 hPa
C_0	Dry gravity wave speed of the baroclinic mode	50 m s^{-1}
ν	Rayleigh friction coefficient	$(10 \text{ day})^{-1}$ in dimensional unit
μ	Newtonian cooling coefficient	$(10 \text{ day})^{-1}$ in dimensional unit
E_k	Nondimensional Ekman number in the BL	0.68
τ	Convective adjustment time	14 h in dimensional unit
α_0	Moisture reference coef	1.5
d	Nondimensional BL depth	0.25
$\overline{Q}$	$\overline{q}_3/d_0$	0.93
$\overline{Q_b}$	$\overline{q}_e/d_0$	1.89
d_0	$d_0 = 2p_2 C_p C_0^2/\Delta p R L_c$	0.008

variables u, v, and Φ represent the low-level zonal wind, meridional wind, and geopotential, respectively (the baroclinic mode of the free troposphere). The variables μ and ν are Newtonian cooling and Rayleigh friction coefficients. The variable q is the column-integrated perturbation moisture and is essentially dominated by the moisture from the surface up to midtroposphere. The variable Pr is precipitation. The variables $\overline{Q}$ and $\overline{Q_b}$ are normalized basic-state specific humidity at the lower-tropospheric layer and the BL, respectively; $\overline{Q}$ and $\overline{Q_b}$ are controlled by the underlying sea surface temperature (SST) (Wang 1988b; Wang and Chen 2016). The variables D and D_b are the lower-tropospheric and BL divergence, respectively. The variables u_b and v_b are BL barotropic winds, and E_k is the friction coefficient in the BL. The variable d is the nondimensional BL depth, which is defined as $d = \Delta P/(P_s - P_e)$ (see Table 1 for definitions of the parameters). Details about the model can be found in Wang and Chen (2016). The standard values for the model parameters are listed in Table 1.

b. WAE precipitation parameterization

Following MS09, the precipitation WAE scheme is assumed to be proportional to the wave activity amplitude,

$$\text{Pr} = \overline{H}\alpha, \tag{7}$$

where α is the perturbation wave activity envelope and $\overline{H}$ is a constant heating rate factor that is determined by the radiative–convective equilibrium, $\overline{R} = \overline{H}\overline{\alpha}$, where $\overline{R} = 1 \text{ K day}^{-1}$ is a constant radiative cooling rate and $\overline{\alpha}$ is a constant amplitude of wave activity in an equilibrium state. To close the parameterization scheme, the perturbation amplitude of the WAE is assumed to be predicted by the linearized equation

$$\frac{\partial \alpha}{\partial t} = \Gamma \overline{\alpha} q_{\text{low}}, \tag{8}$$

where Γq_{low} is the dynamic growth (decay) rate of the WAE and $\Gamma \approx 0.2 \text{ K}^{-1} \text{ day}^{-1}$ in dimensional units, and q_{low} is the low-level moisture. Multiplying $\overline{H}$ on both sides of Eq. (8), we have

$$\frac{\partial \text{Pr}}{\partial t} = \Gamma \overline{R} q_{\text{low}}. \tag{9}$$

Equation (9) means that precipitation tendency is proportional to perturbation low-level moisture. Thus, if we relate q_{low} to q in Eq. (4) (which will be elaborated later), the model Eqs. (1)–(6) and (9) consist of a closed system without knowing α.

c. Simplified Betts–Miller parameterization

For comparison, the simplified Betts–Miller parameterization scheme (Frierson et al. 2004) is adopted in this study. The nondimensional form of the B–M scheme could be expressed as (Wang and Chen 2016)

$$\text{Pr} = \frac{1}{\tau}(q + \alpha_0 \Phi), \tag{10}$$

where τ is the convective adjustment time scale and α_0 is a constant coefficient. The precipitation heating is linearized about the radiative–convective equilibrium (RCE) states.

d. Eigenvalue technique

The eigenvalue technique used in this study is similar to that used in MS09. The precipitation is assumed to be proportional to $\exp(-y^2/2)$, and the long-wave approximation is adopted [neglect time tendency and damping terms in Eq. (2)]. To reduce the complexity of solving
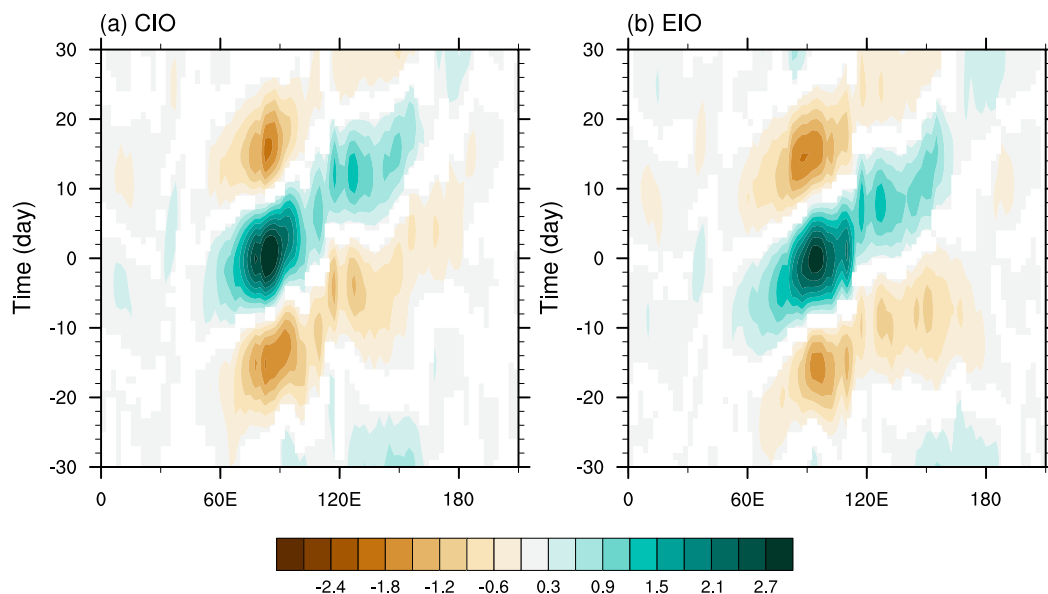
FIG. 1. Propagation of the MJO as depicted by time–lon diagrams of the regressed equatorial precipitation (mm day^{-1}) averaged between 10°S–10°N onto the MJO PIs over the (a) CIO (10°S–10°N, 70°–90°E) and (b) EIO (10°S–10°N, 90°–110°E). Only those significant at 95% level are shown by the color shading. The data used are NDJFM 20–100 filtered daily precipitation. The seasonal cycle and the interannual variability have been removed.

the eigenvalue problem, a stationary BL is used [i.e., the time tendencies in Eqs. (5) and (6) are dropped], and the BL divergence in Eqs. (3) and (4) can be represented in terms of the low-level geopotential (Wang and Rui 1990a; Liu and Wang 2012).

e. Data and methods

The datasets used in this study include the 2.5° × 2.5°, 4-times-daily, ERA-Interim reanalysis data (Dee et al. 2011) for the 18-yr time period from 1998 through 2015. Horizontal wind components, geopotential height, and specific humidity are used in this study. The precipitation data are the daily averaged precipitation from version 7 of the 3B42 product of the Tropical Rainfall Measuring Mission (TRMM; Huffman et al. 2007), based on the period of record from 1998 to 2015.

The data-filtering methods used here are similar to those described in Wheeler and Hendon (2004). First, the time mean and the first three harmonics of the climatological seasonal cycle are removed from the daily field. The interannual variation is then removed by subtracting a previous 120-day running mean. This step can sufficiently remove interannual variation (Lin et al. 2008; Ventrice et al. 2013). In addition, a 20–100-day Lanczos bandpass filtering (Duchon 1979) is applied to all variables. The filtered dataset during November–March (NDJFM) is used in the following sections.

3. Observed structures of the MJO

a. Observed relation between moisture anomaly and precipitation

Motivated by Jiang et al. (2015), we define two precipitation indices (PIs) using equatorial precipitation anomalies averaged between 10°S and 10°N and over the central Indian Ocean (CIO; 70°–90°E) and eastern Indian Ocean (EIO; 90°–110°E). The focus on the Indian Ocean (IO) is because the IO is the key region for the MJO's generation and development. Figure 1 shows the regressed precipitation (averaged between 10°S and 10°N) onto the PIs. It is indicated that the slow eastward-propagation feature (with speed of ~5 m s^{-1}) of the MJO is well reconstructed by using the precipitation indices. Both the diagrams show consistent features of evolution of MJO convection. Thus, the two PIs can be used as references for reconstructing MJO spatial and temporal structures.

Figure 2 shows the vertical structures of the moisture anomaly associated with MJO convection over the two locations defined above. The observed vertical moisture structures are consistent with many previous studies (Sperber 2003; Kiladis et al. 2005; Benedict and Randall 2007; Hsu and Li 2012; Adames and Wallace 2015; Jiang et al. 2015). They show an eastward shift of the positive anomaly in the PBL (below 850 hPa) relative to the convection center. Also evident is the westward vertical tilt of the moisture anomaly in the free atmosphere
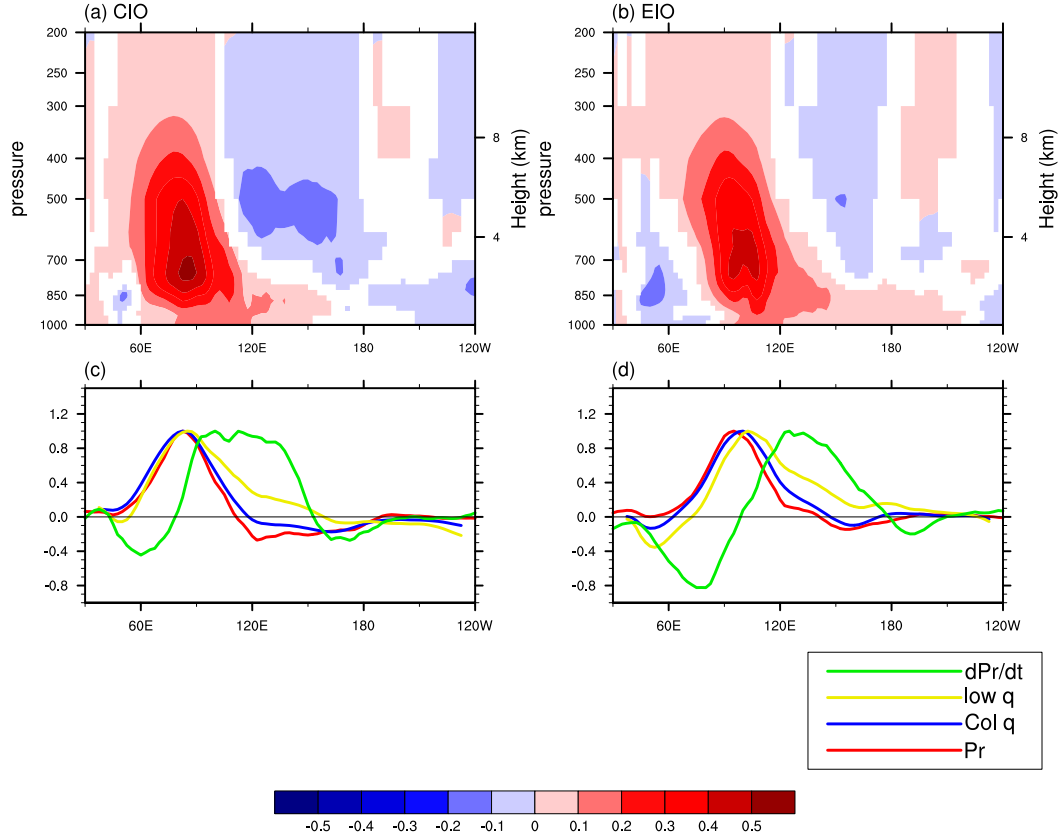
FIG. 2. Vertical structure of moisture (specific humidity; $g\,kg^{-1}$) associated with the MJO. The latitudinally averaged (10°S–10°N) moisture regressed onto precipitation indices over two locations: (a) CIO (70°–90°E) and (b) EIO (90°–110°E). Only those significant at 95% level are shown by color shading. In the line plots are the corresponding regressed MJO precipitation (red line), column-integrated (1000–200 hPa) moisture anomaly (blue line), low-level (defined by Stechmann and Majda 2015) moisture anomaly (yellow line), and precipitation tendency (green line) over (c) CIO and (d) EIO. The precipitation tendency is defined as 2-day centered differential tendency. For comparison, the data used in the line plots are normalized by their respective maximum. The moisture data used are the ERA-Interim for NH winter (NDJFM) during 1998–2015. The precipitation data used are the TRMM 3B42 data (from 1998 to 2015).

(above 850 hPa). Note that the leading PBL moisture anomaly could not be simply interpreted as the downward extension of the westward vertical tilt of the free atmospheric moisture. Thus, it suggests that including BL dynamics may be necessary for theoretical understanding of the MJO.

Equation (9) indicates that the precipitation tendency is proportional to the low-level moisture. Is this relationship supported by observations? Stechmann and Majda (2015) defined the low-level moisture for the MJO skeleton model as the weighted averaged moisture between 925, 850, and 725 hPa. Since the ERA-Interim data do not provide level 725 hPa, we use level 750 hPa instead, and the low-level moisture in this study is defined as

$$q_{low} = 1/4\, q(925\,\text{hPa}) + 1/2\, q(850\,\text{hPa}) + 1/4\, q(750\,\text{hPa}).$$
(11)

Using this definition, Fig. 2 shows the low-level moisture (yellow line) defined by Eq. (11). Also shown are column-integrated moisture (1000–200 hPa, blue line), precipitation (red line), and precipitation tendency (green line). Evidently, the low-level moisture anomaly defined by Stechmann and Majda (2015) is not in phase with the precipitation tendency, indicating that the WAE assumption is inconsistent with the observations.

The phase relation between precipitation and low-level moisture in the WAE scheme can be derived from Eq. (9) by assuming a normal mode solution, $\exp[i(kx - \omega t)]$. Equation (9) then implies

$$-i\omega \text{Pr} = \Gamma \overline{R} q_{low}.$$
(12)

For a neutral mode, where ω is a real number, low-level moisture will be in quadrature with precipitation and leads precipitation for the eastward-moving mode.
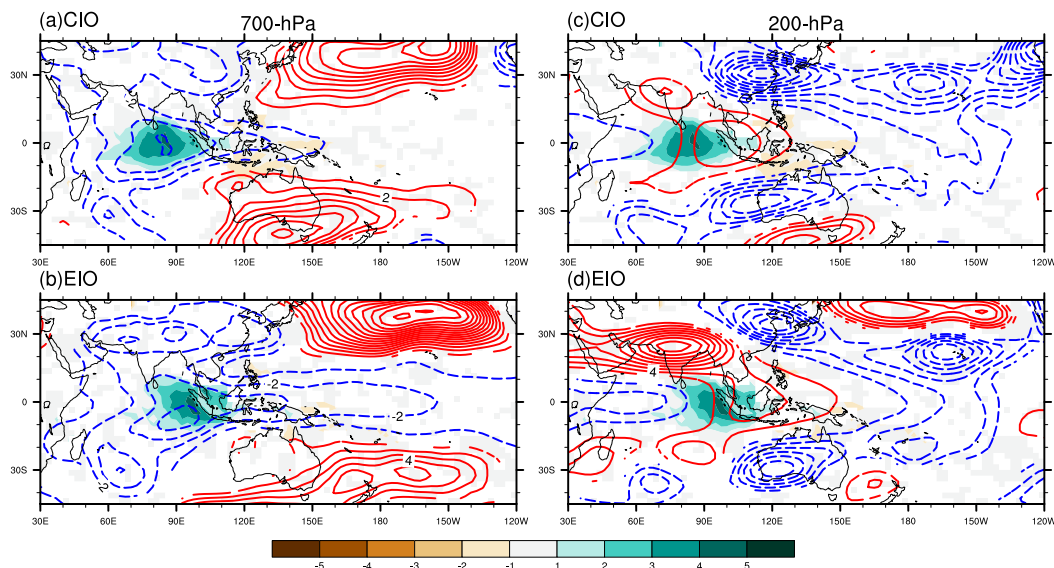
FIG. 3. Observed horizontal structures of the MJO, namely, regressions of geopotential height (m; contours) at (a),(b) 700 hPa and (c),(d) 200 hPa, as well as precipitation (mm day^{-1}; color shading), with respect to the PIs over CIO and EIO regions. Only those significant at 95% level are shown by the color shading and contours. The solid (dashed) contours indicate positive (negative) values. The contour interval is 1 m for 700 hPa and 2 m for 200 hPa.

However, observations show that low-level moisture is not in quadrature phase relation with the precipitation. Rather, the low-level moisture maximum coincides with (Fig. 2c) or only slightly leads (Fig. 2d) the precipitation maximum. Motivated by Yasunaga and Mapes (2012), the phase relation between precipitation and low-level moisture can be obtained by the spectra analysis. Define low-level moisture indices in CIO and EIO regions in the same way as PIs. The spectra analysis indicates that the low-level moisture indices lead the precipitation indices by about 20°–30° for a 30–90-day period in both CIO and EIO regions (results not shown here). Thus, the low-level moisture is not in quadrature (90° phase difference) with the precipitation. Also evident is that low-level moisture to the east of the precipitation maximum decreases slower than column-integrated moisture because of the influence of the leading BL moisture. On the other hand, the MJO precipitation is well correlated with the column-integrated moisture. This result is consistent with many previous studies that water vapor (and relative humidity) is basically in phase with convective activity (Johnson and Ciesielski 2013; Powell and Houze 2013; Sobel et al. 2014; Xu and Rutledge 2014; Adames and Wallace 2015) and the moisture mode theory (Fuchs and Raymond 2005; Sobel and Maloney 2012, 2013; Adames and Kim 2016).

b. Observed horizontal structure

The horizontal lower-level and upper-level circulations associated with the MJO are shown in Fig. 3. It is evident that the low-level (700 hPa) geopotential exhibits a Matsuno–Gill-like pattern (Matsuno 1966; Gill 1980), with a Kelvin-wave low to the east of the convective heating and a pair of equatorial Rossby wave lows to the west. This low-level convectively coupled Kelvin–Rossby wave structure is consistent with results in the previous literature (Rui and Wang 1990; Adames and Wallace 2014a,b).

The geopotential at the upper level (200 hPa) also exhibits a Matsuno–Gill-like pattern with opposite polarity in the vicinity of the convective heating, indicating a first baroclinic convectively coupled mode. However, unlike the low-level pressure pattern, which is trapped within the tropics, the upper-level Rossby waves to the west of the convection are located farther away from the equator with large amplitudes. Also evident is the propagation of wave trains in the subtropics and midlatitudes at both the low level and upper level. The strong upper-level wave trains in the Northern Hemisphere are along the NDJFM westerly jet stream–induced waveguide over the Pacific. The extratropical wave trains over the North Pacific primarily exhibit barotropic structures when convection is centered on EIO. Unlike the low-level circulation, the upper-level circulation shows a quadrupole structure with a cyclone pair to the east of the convection (Fig. 3d). The more complex structure at the upper level and extratropics is partly related to the effects of the NH winter mean flow, especially the jet stream (Monteiro et al. 2014). In summary, the MJO's tropical circulation can be considered as a first baroclinic
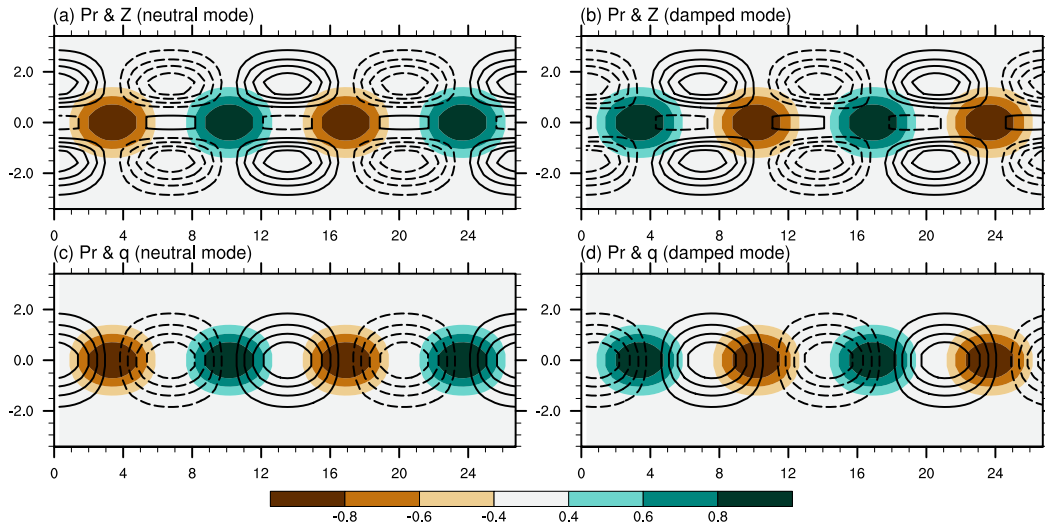
FIG. 4. The horizontal structures of the (a),(c) neutral and (b),(d) damped wavenumber 2 skeleton modes: (a),(b) Show the low-level pressure (contours) and precipitation (color shading); (c),(d) Show the corresponding low-level specific humidity (contours) and precipitation (color shading). All fields are normalized by their respective maximum values. The solid (dashed) contours indicate positive (negative) values. The contour interval is 0.2 for all panels. The zero contour is omitted. Moisture is shown for only the lowest meridional mode. The phase speeds for the neutral and damped skeleton mode are 4.9 and 4.6 m s^{-1}, respectively. The decay rate for the damped skeleton mode is 0.05 day^{-1}.

convectively coupled Kelvin–Rossby wave structure that resembles the Matsuno–Gill pattern.

4. Examination of the effect and deficiency of the WAE parameterization

a. Skeleton mode without BL

In the general MJO theoretical framework, the moisture variable is defined as the column-integrated moisture. In a two-layer atmospheric model, the vertical integrated moisture content approximately equals the vertical integrated moisture from 1000 to 500 hPa or could be even approximated by the low-level moisture. With this approximation, we can use the WAE scheme in this general MJO framework. Note that without the BL dynamics (by setting the BL depth d to zero), Eq. (4) reduces to the same form as the skeleton model of MS09. When the SST is chosen as 28.0°C, the coefficient $\overline{Q}$ is 0.93, which is comparable to the values used in MS09. In this sense, our model framework could be reduced to MS09 if the BL dynamic is excluded.

First, we considered the neutral mode. The neutral mode is obtained by setting the damping (Newtonian cooling and Rayleigh friction) to zero. The low-level structure of the neutral skeleton mode is shown in Fig. 4a. Corresponding to the convective heating, there is a Kelvin-wave response to the east and Rossby-wave response to the west. However, unlike the canonical

Matsuno–Gill pattern, the Kelvin-wave low is out of phase with the Rossby-wave lows. This makes the Kelvin wave appear to be muted with respect to the Rossby wave component. This so-called "quadrupole" horizontal structure is inconsistent with the observed low-level pressure (geopotential height) pattern shown in Fig. 3. The observation clearly shows a convectively coupled Kelvin–Rossby wave structure that resembles the Matsuno–Gill pattern, while the neutral skeleton mode does not.

The reason that the neutral mode produces this out-of-phase relation between Kelvin and Rossby waves is due to the absence of damping in the model. The damping could damp the Kelvin and Rossby waves as they propagate away from the precipitation heat source, which would lead to the canonical Matsuno–Gill pattern. This point is demonstrated in the study of Adames and Kim (2016). Motivated by their study, we turn on the Newtonian cooling and Rayleigh friction, with a 10-day damping time scale. Figure 4b shows the structure of the corresponding damped skeleton mode. It is evident that with damping, the precise out-of-phase relation between Kelvin and Rossby waves is altered, and the skeleton mode shows a low-level structure that more resembles the Matsuno–Gill pattern.

The relation between precipitation and the low-level moisture anomaly for the neutral skeleton mode is shown in Fig. 4c. Obviously, the neutral skeleton mode produces a quadrature relation between moisture and

precipitation, and precipitation lags moisture by a quarter of a wavelength, as predicted by Eq. (12). This phase relation is inconsistent with the observed phase relation between low-level moisture and precipitation shown in Fig. 2. Note that the maximum low-level moisture shifts farther eastward from the precipitation maximum in the damped skeleton mode (Fig. 4d). This is actually the consequence of the negative growth rate (*e*-folding time scale is about 20 days). For a damping mode, $\omega = \omega_r + i\omega_i$ is a complex number, and ω_i is negative. Thus, according to Eq. (12), the phase lag between maximum low-level moisture and maximum precipitation will be larger than a quarter of a wavelength. Note that if ω_i is positive (i.e., unstable mode), the phase lag between low-level moisture and precipitation will be reduced.

b. Frictional skeleton mode with BL

Recall that instability could reduce the phase lag between precipitation and low-level moisture. It is interesting to ask whether the MJO-like mode could produce both a more realistic horizontal structure and reasonable precipitation–moisture relation if an instability mechanism is introduced. Given that the BL frictional convergence could lead to instability (Wang and Rui 1990a; Wang and Li 1994; Liu and Wang 2012), it is worth reexamining the WAE scheme by including the BL dynamics (by turning on the BL depth *d*).

With the stationary BL dynamics assumption [neglecting time tendencies in Eqs. (5) and (6)], the eigenvalue problem is easily solved. The Newtonian and Rayleigh damping time scales are set to be 10 days. The propagation speed for the MJO-like mode is roughly $6.2 \, \text{m s}^{-1}$, which is comparable to Liu and Wang (2012). The *e*-folding time scale growth rate of the MJO energy is about 11 days. It is consistent with the result of Liu and Wang (2012) that the frictional skeleton model could produce an unstable eastward-moving mode.

The horizontal structure of the MJO-like skeleton mode is shown in Fig. 5. The horizontal low-level geopotential pattern (Fig. 5a) for the simulation of the MJO-like mode shows the more realistic Matsuno–Gill pattern (Matsuno 1966; Gill 1980), with a Kelvin wave to the east of the WAE (precipitation heating) and a Rossby wave to the west. This pattern also resembles the "quadrupole" structure to some extent. The quadrupole vortex feature has been documented in previous studies (Rui and Wang 1990; Hendon and Salby 1994; Kiladis et al. 2005). The result here suggests that a wavelike (or a dipolar) heat pattern can produce the quadrupole structure.

What is the phase relationship between the precipitation anomaly and moisture anomaly in the presence of BL dynamics? The precipitation, low-level moisture, and BL convergence are shown in Fig. 5b. The most notable feature is that the quadrature phase lag between low-level moisture and precipitation has been reduced. However, the phase lag is still large compared to observations given the fact that the maximum low-level moisture coincides with or only slightly leads the maximum precipitation (Figs. 2c,d). Also notable is that the BL convergence leads the precipitation.

Why did instability fail to change the precipitation–moisture relationship significantly? According to Eq. (12), if the growth rate is moderate (*e*-folding time scale of 11 days), the phase lag between precipitation and moisture will not be significantly changed. Only when the growth rate is strong (ω_i is large) or the frequency is low (ω_r is small), the phase lag between precipitation and low-level moisture in the model solution may be reduced significantly and approach the observations. In that case, either the propagation speed is unrealistically too small or the growth rate is unrealistically too large. This deficiency is the consequence of the WAE assumption [Eq. (9)].

5. Comparison to MJO theories with simplified Betts–Miller scheme

Since the major deficiency of the WAE scheme is the erroneous assumption on the moisture–precipitation relation, it is interesting and necessary to compare the MJO skeleton theory to those models that correctly depict the precipitation–moisture relation. The simplified Betts–Miller-type parameterization used in the "moisture mode" theory (Sobel and Maloney 2012, 2013; Adames and Kim 2016) correctly depicts the in-phase relation between precipitation and column-integrated moisture. Adames and Kim (2016) extended the moisture mode theory by treating the meridional structure of the basic equation explicitly. Their model successfully produced an MJO-like mode with dispersion relation close to the observations. Compared with the WAE scheme and the skeleton model, their results also showed the more realistic Matsuno–Gill-like horizontal pattern with a planetary-scale zonal selection when damping terms are turned on. Their results also showed planetary instability for the MJO.

Similar to the moisture mode theory, Wang and Chen (2016) extended the frictional convergence theory (Wang and Rui 1990a; Wang and Li 1994) to trio-interaction theory by including moisture feedback and the simplified Betts–Miller scheme. Their model framework includes Eqs. (1)–(6) and the simplified Betts–Miller scheme [Eq. (10)]. Here, we make
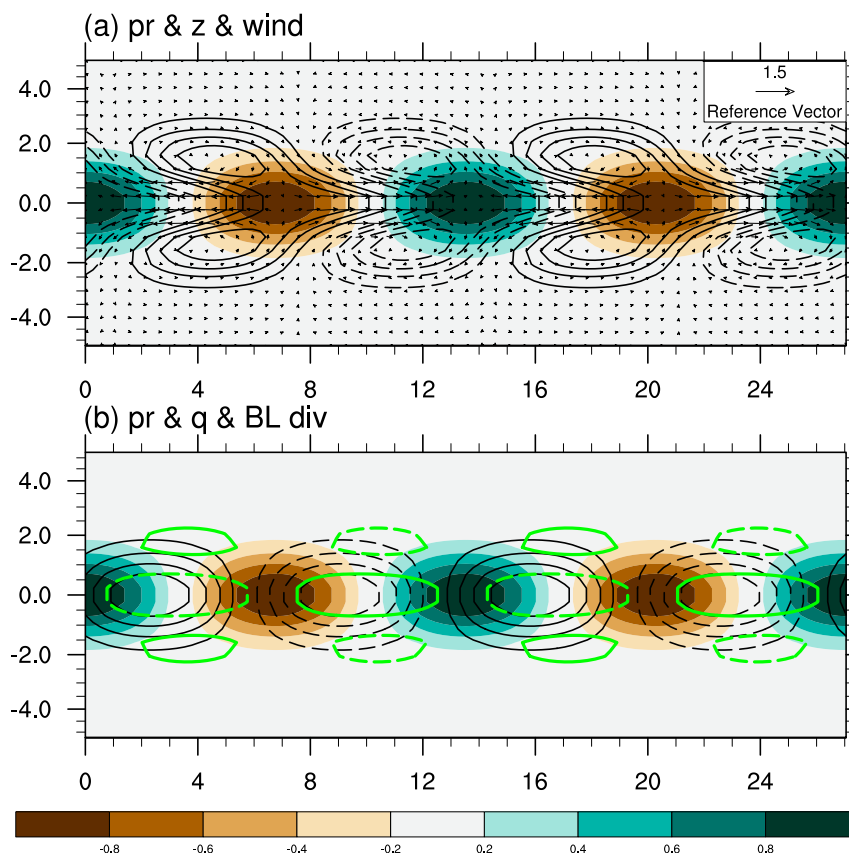
FIG. 5. Wavenumber 2 frictional skeleton mode: (a) geopotential (contours), wind (vectors), and precipitation (color shading); (b) low-level moisture (contours) and precipitation (color shading). The green contours in (b) indicate the locations (with normalized amplitudes exceeding 0.4) of BL divergence (solid lines indicate divergence, and dashed lines indicate convergence). The moisture is shown for only the lowest meridional mode. All fields are normalized by their respective maximum (absolute) values. The wind vectors are normalized by the largest wind speed. The solid (dashed) contours indicate positive (negative) values. The contour interval is 0.2 for both panels. The zero contour is omitted. The propagation speed is $6.2 \, \text{m s}^{-1}$, and the growth rate is $0.09 \, \text{day}^{-1}$.

a comparison between the MJO-like mode with the simplified Betts–Miller scheme and the frictional skeleton mode (Fig. 5). To be consistent with Fig. 5, the precipitation is again assumed to be proportional to $\exp(-y^2/2)$. We also return the definition of q to the column-integrated moisture. An additional radiative feedback process is [Eq. (3)] by adding $R = -\gamma \text{Pr}$ (with $\gamma = 0.2$) to the right-hand side of Eq. (3) since Adames and Kim (2016) showed that radiative–convective feedback is important for MJO intensification.

The MJO-like mode with the simplified Betts–Miller scheme exhibits slow eastward propagation ($\sim 6.4 \, \text{m s}^{-1}$) and unstable growth with e-folding time scale of 10 days when the SST is 29°C ($\overline{Q}$ is 0.98 and $\overline{Q}_b$ is 1.98) and the convective time scale τ is 14 h. The simulated low-level horizontal structure of the MJO-like mode is shown in

Fig. 6a. The simulated MJO-like mode well captures the horizontal features of the MJO low-level circulation, which is evident as a convectively coupled Kelvin–Rossby wave structure. Furthermore, the model captures a realistic precipitation–moisture relationship (Fig. 6b); that is, the BL moisture convergence leads precipitation and column-integrated moisture coincides with precipitation.

6. Conclusions and discussion

The WAE convective scheme for theoretical modeling of the MJO was reexamined by using observational data and the general MJO theoretical framework developed by Wang and Chen (2016). The WAE convective scheme assumes that the precipitation tendency is proportional to the low-level moisture. Under this
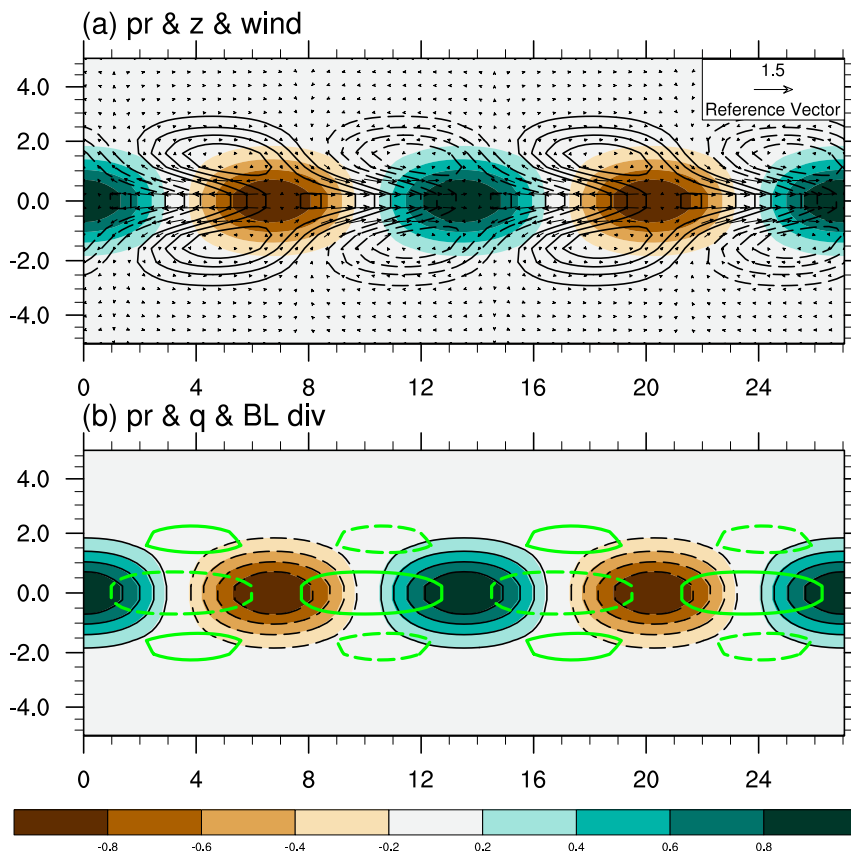
FIG. 6. As in Fig. 5, but for wavenumber 2 MJO-like mode with the simplified B–M scheme. The propagation speed is $6.4\,\mathrm{m\,s^{-1}}$, and the growth rate is $0.1\,\mathrm{day^{-1}}$.

assumption, the neutral skeleton mode produces a quadrature phase relation between precipitation and low-level moisture. The observation shows that the precipitation tendency is not in phase with the low-level moisture; the precipitation is in phase with the column-integrated moisture and lead by the boundary layer moisture convergence. Also, the precipitation is not in quadrature with low-level moisture. The WAE assumption is inconsistent with observations while the moisture mode theory and trio-interaction theory are consistent with the observed vertical moisture structure.

The observation also shows that the low-level MJO circulation is a convectively coupled Kelvin–Rossby (a Matsuno–Gill-like) pattern. The horizontal structure of the neutral skeleton mode is inconsistent with observations. Including damping terms could lead to a pattern slightly more similar to the Matsuno–Gill pattern, but the mode is damped. By including the BL dynamics, the model produces an unstable mode with improved horizontal circulation structure and moisture–precipitation relation, but the deficiency in the moisture–precipitation relation remains. The latter is due to the deficiency of the WAE scheme. As a

conclusion, while the general MJO theoretical framework with the WAE scheme could produce realistic eastward phase speed, it fails to produce a realistic precipitation–moisture relation. On the other hand, the general model with the simplified B–M scheme produces a realistic horizontal structure (coupled Kelvin–Rossby wave structure) and vertical moisture structure (i.e., the BL moisture convergence leads precipitation, and precipitation coincides with column-integrated moisture).

This study suggests that although obtaining reasonable eastward propagation and dispersion features may be important for theoretical modeling of the MJO, it is just as important for the theoretical MJO model to produce a correct precipitation–moisture relation as well as the horizontal circulation structures. As suggested by Wang and Chen (2016), the essence of the MJO that requires theoretical explanation includes 1) the coupled Kelvin–Rossby wave (horizontal) structure that is similar to the Matsuno–Gill pattern; 2) the slow eastward propagation (about $5\,\mathrm{m\,s^{-1}}$); 3) the planetary zonal circulation scale (planetary zonal selection); 4) the PBL moisture convergence leading the major convection center and

backward-tilted vertical structure; and 5) growth (decay) in the warm (cold) oceans. These essential features may be viewed as major targets for theoretical interpretation and validation metrics of MJO theory.

REFERENCES

Adames, Á. F., and J. M. Wallace, 2014a: Three-dimensional structure and evolution of the vertical velocity and divergence fields in the MJO. *J. Atmos. Sci.*, **71**, 4661–4681, doi:10.1175/JAS-D-14-0091.1.

——, and ——, 2014b: Three-dimensional structure and evolution of the MJO and its relation to the mean flow. *J. Atmos. Sci.*, **71**, 2007–2026, doi:10.1175/JAS-D-13-0254.1.

——, and ——, 2015: Three-dimensional structure and evolution of the moisture field in the MJO. *J. Atmos. Sci.*, **72**, 3733–3754, doi:10.1175/JAS-D-15-0003.1.

——, and D. Kim, 2016: The MJO as a dispersive, convectively coupled moisture wave: Theory and observations. *J. Atmos. Sci.*, **73**, 913–941, doi:10.1175/JAS-D-15-0170.1.

Benedict, J. J., and D. A. Randall, 2007: Observed characteristics of the MJO relative to maximum rainfall. *J. Atmos. Sci.*, **64**, 2332–2354, doi:10.1175/JAS3968.1.

Betts, A. K., 1986: A new convective adjustment scheme. Part I: Observational and theoretical basis. *Quart. J. Roy. Meteor. Soc.*, **112**, 677–691, doi:10.1002/qj.49711247307.

——, and M. J. Miller, 1986: A new convective adjustment scheme. Part II: Single column tests using GATE wave, BOMEX, ATEX and Arctic air-mass data sets. *Quart. J. Roy. Meteor. Soc.*, **112**, 693–709, doi:10.1002/qj.49711247308.

Dee, D. P., and Coauthors, 2011: The ERA-Interim reanalysis: Configuration and performance of the data assimilation system. *Quart. J. Roy. Meteor. Soc.*, **137**, 553–597, doi:10.1002/qj.828.

Duchon, C. E., 1979: Lanczos filtering in one and two dimensions. *J. Appl. Meteor.*, **18**, 1016–1022, doi:10.1175/1520-0450(1979)018<1016:LFIOAT>2.0.CO;2.

Emanuel, K. A., 1987: An air–sea interaction model of intraseasonal oscillations in the tropics. *J. Atmos. Sci.*, **44**, 2324–2340, doi:10.1175/1520-0469(1987)044<2324:AASIMO>2.0.CO;2.

Frierson, D. M. W., A. J. Majda, and O. M. Pauluis, 2004: Large scale dynamics of precipitation fronts in the tropical atmosphere: A novel relaxation limit. *Commun. Math. Sci.*, **2**, 591–626, doi:10.4310/CMS.2004.v2.n4.a3.

Fuchs, Z., and D. J. Raymond, 2005: Large-scale modes in a rotating atmosphere with radiative–convective instability and WISHE. *J. Atmos. Sci.*, **62**, 4084–4094, doi:10.1175/JAS3582.1.

Gill, A. E., 1980: Some simple solutions for heat-induced tropical circulation. *Quart. J. Roy. Meteor. Soc.*, **106**, 447–462, doi:10.1002/qj.49710644905.

Hendon, H. H., and M. L. Salby, 1994: The life cycle of the Madden–Julian oscillation. *J. Atmos. Sci.*, **51**, 2225–2237, doi:10.1175/1520-0469(1994)051<2225:TLCOTM>2.0.CO;2.

Hsu, P.-C., and T. Li, 2012: Role of the boundary layer moisture asymmetry in causing the eastward propagation of the Madden–Julian oscillation. *J. Climate*, **25**, 4914–4931, doi:10.1175/JCLI-D-11-00310.1.

Huffman, G. J., and Coauthors, 2007: The TRMM Multisatellite Precipitation Analysis (TMPA): Quasi-global, multiyear, combined-sensor precipitation estimates at fine scales. *J. Hydrometeor.*, **8**, 38–55, doi:10.1175/JHM560.1.

Jiang, X., and Coauthors, 2015: Vertical structure and physical processes of the Madden–Julian oscillation: Exploring key model physics in climate simulations. *J. Geophys. Res. Atmos.*, **120**, 4718–4748, doi:10.1002/2014JD022375.

Johnson, R. H., and P. E. Ciesielski, 2013: Structure and properties of Madden–Julian oscillations deduced from DYNAMO sounding arrays. *J. Atmos. Sci.*, **70**, 3157–3179, doi:10.1175/JAS-D-13-065.1.

Kang, I.-S., F. Liu, M.-S. Ahn, Y.-M. Yang, and B. Wang, 2013: The role of SST structure in convectively coupled Kelvin–Rossby waves and its implications for MJO formation. *J. Climate*, **26**, 5915–5930, doi:10.1175/JCLI-D-12-00303.1.

Kiladis, G. N., K. H. Straub, and P. T. Haertel, 2005: Zonal and vertical structure of the Madden–Julian oscillation. *J. Atmos. Sci.*, **62**, 2790–2809, doi:10.1175/JAS3520.1.

Kuo, H.-L., 1974: Further studies of the parameterization of the influence of cumulus convection on large-scale flow. *J. Atmos. Sci.*, **31**, 1232–1240, doi:10.1175/1520-0469(1974)031<1232:FSOTPO>2.0.CO;2.

Lau, K.-M., and L. Peng, 1987: Origin of low-frequency (intraseasonal) oscillations in the tropical atmosphere. Part I: Basic theory. *J. Atmos. Sci.*, **44**, 950–972, doi:10.1175/1520-0469(1987)044<0950:OOLFOI>2.0.CO;2.

Lin, J.-L., M.-I. Lee, D. Kim, I.-S. Kang, and D. M. W. Frierson, 2008: The impacts of convective parameterization and moisture triggering on AGCM-simulated convectively coupled equatorial waves. *J. Climate*, **21**, 883–909, doi:10.1175/2007JCLI1790.1.

Liu, F., and B. Wang, 2012: A frictional skeleton model for the Madden–Julian oscillation. *J. Atmos. Sci.*, **69**, 2749–2758, doi:10.1175/JAS-D-12-020.1.

Majda, A. J., and S. N. Stechmann, 2009: The skeleton of tropical intraseasonal oscillations. *Proc. Natl. Acad. Sci. USA*, **106**, 8417–8422, doi:10.1073/pnas.0903367106.

Maloney, E. D., and D. L. Hartmann, 1998: Frictional moisture convergence in a composite life cycle of the Madden–Julian oscillation. *J. Climate*, **11**, 2387–2403, doi:10.1175/1520-0442(1998)011<2387:FMCIAC>2.0.CO;2.

Matsuno, T., 1966: Quasi-geostrophic motions in the equatorial area. *J. Meteor. Soc. Japan*, **44**, 25–43. [Available online at https://www.jstage.jst.go.jp/article/jmsj1965/44/1/44_1_25/_pdf.]

Monteiro, J. M., Á. F. Adames, J. M. Wallace, and J. S. Sukhatme, 2014: Interpreting the upper level structure of the Madden–Julian oscillation. *Geophys. Res. Lett.*, **41**, 9158–9165, doi:10.1002/2014GL062518.

Neelin, J. D., I. M. Held, and K. H. Cook, 1987: Evaporation–wind feedback and low-frequency variability in the tropical atmosphere. *J. Atmos. Sci.*, **44**, 2341–2348, doi:10.1175/1520-0469(1987)044<2341:EWFALF>2.0.CO;2.

Powell, S. W., and R. A. Houze Jr., 2013: The cloud population and onset of the Madden–Julian oscillation over the Indian Ocean

during DYNAMO-AMIE. *J. Geophys. Res. Atmos.*, **118**, 11 979–11 995, doi:10.1002/2013JD020421.

Rui, H., and B. Wang, 1990: Development characteristics and dynamic structure of tropical intraseasonal convection anomalies. *J. Atmos. Sci.*, **47**, 357–379, doi:10.1175/1520-0469(1990)047<0357:DCADSO>2.0.CO;2.

Sobel, A., and E. Maloney, 2012: An idealized semi-empirical framework for modeling the Madden–Julian oscillation. *J. Atmos. Sci.*, **69**, 1691–1705, doi:10.1175/JAS-D-11-0118.1.

——, and ——, 2013: Moisture modes and the eastward propagation of the MJO. *J. Atmos. Sci.*, **70**, 187–192, doi:10.1175/JAS-D-12-0189.1.

——, S. Wang, and D. Kim, 2014: Moist static energy budget of the MJO during DYNAMO. *J. Atmos. Sci.*, **71**, 4276–4291, doi:10.1175/JAS-D-14-0052.1.

Sperber, K. R., 2003: Propagation and the vertical structure of the Madden–Julian oscillation. *Mon. Wea. Rev.*, **131**, 3018–3037, doi:10.1175/1520-0493(2003)131<3018:PATVSO>2.0.CO;2.

Stechmann, S. N., and A. J. Majda, 2015: Identifying the skeleton of the Madden–Julian oscillation in observational data. *Mon. Wea. Rev.*, **143**, 395–416, doi:10.1175/MWR-D-14-00169.1.

Thual, S., A. J. Majda, and S. N. Stechmann, 2014: A stochastic skeleton model for the MJO. *J. Atmos. Sci.*, **71**, 697–715, doi:10.1175/JAS-D-13-0186.1.

Tian, B., D. E. Waliser, E. J. Fetzer, B. H. Lambrigtsen, Y. L. Yung, and B. Wang, 2006: Vertical moist thermodynamic structure and spatial–temporal evolution of the MJO in AIRS observations. *J. Atmos. Sci.*, **63**, 2462–2485, doi:10.1175/JAS3782.1.

Ventrice, M. J., M. C. Wheeler, H. H. Hendon, C. J. Schreck, C. D. Thorncroft, and G. N. Kiladis, 2013: A modified multivariate Madden–Julian oscillation index using velocity potential. *Mon. Wea. Rev.*, **141**, 4197–4210, doi:10.1175/MWR-D-12-00327.1.

Wang, B., 1988a: Comments on "An air–sea interaction model of intraseasonal oscillation in the tropics." *J. Atmos. Sci.*, **45**, 3521–3525, doi:10.1175/1520-0469(1988)045<3521:COAIMO>2.0.CO;2.

——, 1988b: Dynamics of tropical low-frequency waves: An analysis of the moist Kelvin wave. *J. Atmos. Sci.*, **45**, 2051–2065, doi:10.1175/1520-0469(1988)045<2051:DOTLFW>2.0.CO;2.

——, and H. Rui, 1990a: Dynamics of the coupled moist Kelvin–Rossby wave on an equatorial β-plane. *J. Atmos. Sci.*, **47**, 397–413, doi:10.1175/1520-0469(1990)047<0397:DOTCMK>2.0.CO;2.

——, and ——, 1990b: Synoptic climatology of transient tropical intraseasonal convection anomalies: 1975–1985. *Meteor. Atmos. Phys.*, **44**, 43–61, doi:10.1007/BF01026810.

——, and T. Li, 1994: Convective interaction with boundary-layer dynamics in the development of a tropical intraseasonal system. *J. Atmos. Sci.*, **51**, 1386–1400, doi:10.1175/1520-0469(1994)051<1386:CIWBLD>2.0.CO;2.

——, and F. Liu, 2011: A model for scale interaction in the Madden–Julian oscillation. *J. Atmos. Sci.*, **68**, 2524–2536, doi:10.1175/2011JAS3660.1.

——, and G. Chen, 2016: A general theoretical framework for understanding essential dynamics of Madden–Julian oscillation. *Climate Dyn.*, doi:10.1007/s00382-016-3448-1, in press.

Wheeler, M. C., and H. H. Hendon, 2004: An all-season real-time multivariate MJO index: Development of an index for monitoring and prediction. *Mon. Wea. Rev.*, **132**, 1917–1932, doi:10.1175/1520-0493(2004)132<1917:AARMMI>2.0.CO;2.

Xu, W., and S. A. Rutledge, 2014: Convective characteristics of the Madden–Julian oscillation over the central Indian Ocean observed by shipborne radar during DYNAMO. *J. Atmos. Sci.*, **71**, 2859–2877, doi:10.1175/JAS-D-13-0372.1.

Yasunaga, K., and B. Mapes, 2012: Differences between more divergent and more rotational types of convectively coupled equatorial waves. Part I: Space–time spectral analyses. *J. Atmos. Sci.*, **69**, 3–16, doi:10.1175/JAS-D-11-033.1.